Journal of Electronics and Electrical Engineering
https://ojs.wiserpub.com/index.php/JEEE

UNIVERSAL WISER PUBLISHER

Research Article

Dynamic Simulation of a DC Microgrid for a Remote Community in Ghana

Godfred Atinkum*, M. Tariq Iqbal, John E. Quaicoe

Department of Electrical and Computer Engineering, Memorial University of Newfoundland, St. Johns, NL, Canada
E-mail: godredatinkum14@gmail.com

Received: 14 July 2025; **Revised:** 18 September 2025; **Accepted:** 23 September 2025

Abstract: Microgrids are a growing solution for providing sustainable energy to remote communities. However, the complex mix of different sources requires careful analysis of their behavior over time. This paper presents dynamic modeling and simulation of a DC microgrid for a remote Ghanaian community. The system integrates a photovoltaic system, a wind generation system, a diesel generator, power converters, and a battery energy storage system, all of which are connected to a common DC bus. Component selection and system sizing were performed in Homer Pro. A detailed component-level model of the system is developed using MATLAB/Simulink to capture its transient behavior. Two maximum power point tracking techniques are used to optimize power extraction from the PV and wind generation systems, respectively. Simulated results include the responses observed for the components' voltage, current, and power waveforms under varying solar irradiation, wind, and changing load conditions. The dynamic simulations demonstrate effective voltage regulation, load adaptability, and system stability in response to changes in solar irradiance, wind speeds, and load changes.

***Keywords*:** dynamic simulation, hybrid power system, Incremental Conductance (INC), Maximum Power Point Tracking (MPPT), microgrid, renewable energy

1. Introduction

Microgrids (MGs) are becoming increasingly popular in delivering reliable and efficient energy to remote communities worldwide. A common practice is integrating different generation sources to achieve optimum performance, reliability, and cost amid weather and seasonal fluctuations. The unique architecture of combining distributed energy resources (DERs), storage systems, and variable loads within a confined electrical network creates operational complexities that are not encountered in traditional power grids. It is thus essential to analyze the time-varying behavior of an MG under different operating conditions, as an understanding of the dynamic response is key to ensuring stability, reliability, and operational efficiency.

Unlike conventional power systems, MGs are typically dominated by power electronic interfaces with low inertia and fast dynamic responses. Although there are similarities in the components' modelling and analysis [1], traditional power systems' conventional quasi-static phasor models are often insufficient. Therefore, more detailed dynamic modelling approaches are required to capture MGs' behavior accurately. This makes MGs' dynamic behavior fundamentally different from traditional power systems.

DOI: https://doi.org/10.37256/jeee.4220257851

Accurate dynamic modelling of MGs is a critical prerequisite for their reliable design and operation. The diversity of components, ranging from inverter-dominated DERs to energy storage systems and responsive loads, introduces nonlinearities, fast transients, and stability issues that need to be addressed [2]. As a result, researchers have increasingly turned to time-domain simulation tools and detailed converter-level models to study transient behavior, stability margins, and control performance. Several tools and platforms have been developed to perform dynamic simulations of microgrids. MATLAB/Simulink is one of the most widely used environments due to its flexibility in building custom models and controllers [3]. PSCAD/EMTDC provides detailed electromagnetic transient and stability simulation [4, 5], while DIgSILENT PowerFactory offers strong support for steady-state and dynamic analysis of larger microgrid systems [6, 7]. Additionally, real-time simulators like OPAL-RT and field programmable gate arrays enable hardware-in-the-loop testing, where actual controllers are interfaced with simulated microgrids to validate their performance under realistic dynamic conditions [8].

Previous research has investigated the dynamic modeling and analysis of hybrid power systems. A framework for dynamically modelling DC MGs was presented by Castro et al. in [9]. The study designed the components using a lumped parameter modelling approach, which was implemented in Simulink. The results revealed that the high-frequency dynamics of switching devices and converters due to disturbances were absent.

In a related work, Etoju and Farzaneh [10] used optimization to design and simulate a photovoltaic thermal (PV/T), wind, and battery MG. Their modelling approach involved formulating a mathematical problem to determine the optimal system components. They simulated their model for 72 hours and compared the results with a PV/wind/battery system. Results from their simulation showed that their PV/T -based MG edged the PV-based system under cloudy and rainy seasons. They further improved battery system operation performance by nearly 1.8Wh.

Most of the simulation studies have used different techniques, including control [11] and power management [8, 12] to simulate and analyze the dynamic behavior of MGs. The control techniques are used to extract maximum power from the MG components. For example, Mwaka et al. [13] used a perturb and observe (P&O) based MPPT with a PI controller to control the DC bus voltage and extract maximum power. A similar control scheme is presented in [14]. In contrast to the approach used in [13], the authors in [14] used bulk and float charging strategies for their BESS below and above 85% SoC, respectively. The dynamic simulation produced waveforms with less than 1% total harmonic distortion. Jiang and Iqbal [15] simulated a hybrid power system for a rural community in China. The authors used an incremental conductance MPPT with a charge control function to control the duty cycle of a boost converter. Their approach resulted in a stable rms load voltage with ±2 V oscillations around the mean value. On the other hand, the system's DC voltage showed noticeable oscillations.

Nair and Ponnusamy [16] proposed a variable droop control strategy for a standalone DC MG. The aim was to share the load between two inverters optimally. The system was simulated using load transients of 1.5kW at 0.25s, 0.5s, and 0.8s, and the results were compared with a fixed droop control system. They achieved an equal current sharing between the inverters and an improved voltage regulation of 0.73% over a fixed drop control system.

Power management techniques, on the other hand, are used to maintain stability by keeping voltage and frequency within acceptable limits, irrespective of the MG mode of operation [17]. A power management and a power curtailment PV control scheme were presented in [8] to operate a standalone MG. The authors used a DC-link voltage regulation scheme to maintain power balance in the system and transition the MG from generation to load mode. Similarly, in reference [12], a model predictive control-based energy management strategy is proposed to minimize uncertainties and provide power stability from renewable sources in islanded multi-MGs.

Building upon the methodologies and findings in previous studies, it becomes evident that dynamic simulation plays an essential role in analyzing MGs. As MGs become more complex, there is a need for an end-to-end dynamic model that can simulate the interactions between subsystems in a coordinated manner. The goal of this work is to build, simulate, and verify a dynamic model of the DC hybrid power system presented in [18]. A detailed time-domain simulation model is developed using MATLAB/Simulink to capture and analyze the system's transient behavior effectively. The rest of the work is organized as follows: Section 2 presents the system under study and modelling of the components. The dynamic simulation of the proposed system is presented in Section 3. Section 4 discusses the simulation results, and Section 5 concludes the study.

2. Case study and modelling of the components

This research builds upon prior studies conducted by Atinkum et al. [18] on DC microgrid sizing and modeling to enhance the understanding of dynamic behavior under varying load and generation conditions. The previous work applied HOMER to size the microgrid and determine optimal component configuration for a remote community known as Azizakpe in Ghana. The current study extends these models by incorporating dynamic simulation and control techniques to evaluate the system's transient behavior.

According to the findings in [18], the estimated annual average energy demand per house is 912.5 kWh. The typical solar irradiation and wind speed for the area are 5.06 kWh/m^2/day and 4.79 m/s respectively.

For 107 households, the study determined that a combination of 102 kW solar energy, 24.3 kW wind energy, 30 kW diesel power, and 290 kWh battery energy storage system would efficiently meet the village's energy demand. Table 1 lists electricity consumption and load contributed by typical household appliances in Azizakpe, and Figure 1 depicts the system architecture.

Table 1. Household load estimation

Equipment	Average rating (kW)	Average number per household	Hours of use per day	Average energy demand (kWh/day)
Light bulb	0.01	5	6	0.3
Television set	0.05	1	8	0.4
Fan	0.017	2	8	0.3
Refrigerator	0.1	1	12	1.2
Electric iron	1.2	1	0.25	0.3

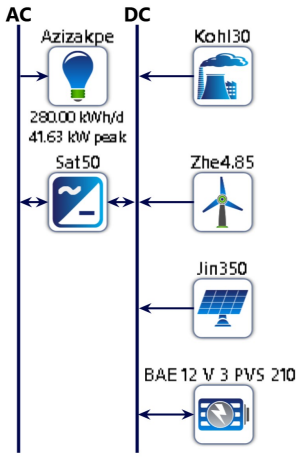

Figure 1. Architecture of the proposed system

It was determined in reference [18] that the system has capital, net present, and operating costs of $133,275.00, $250,689.00, and $4,696.54, respectively. Its levelized cost of energy (LCOE) is $0.09812 and has a simple payback period of approximately 7 years with a 35.4% return on investment. With an estimated yearly CO_2 emission of 1,488kg, the system achieves a 98.6% renewable fraction.

Microgrid System Components Modelling

1. Photovoltaic System

PV modules comprise several cells connected in series and parallel to generate DC power from solar energy. The cell's I-V characteristics in Figure 2 are defined by the following equations for a single diode [19]:

$$I_d = I_{sc}\left[\exp\left(\frac{V_d}{V_T}\right) - 1\right] \tag{1}$$

Here, the thermal voltage V_T equal to,

$$V_T = \frac{kT}{q} \times nI \times N_{cell} \tag{2}$$

From the single diode equivalent circuit model shown in Figure 3 [19], the light-generated current source is antiparallel to the diode. The series resistance, R_s, and shunt resistance, R_{sh} contribute to the losses in the PV cell. Using this model, the cell's output current

$$I = I_L - I_d \tag{3}$$

In the preceding equations, I_d is the diode current (A), I_L is the photocurrent, V_d is the diode voltage (V), I_{sc} is the diode saturation current, nI is the diode ideality factor, k is the Boltzmann constant, q is the electron charge, T is the cell temperature, and N_{cell} is the number of cells connected in series.

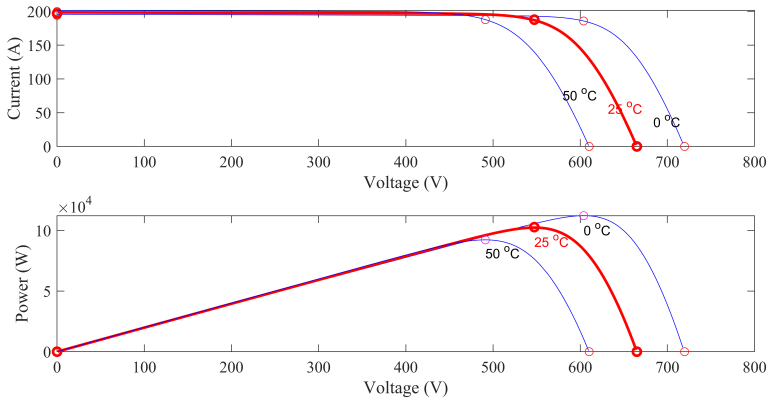

Figure 2. Jinko solar array I-V and P-V curve

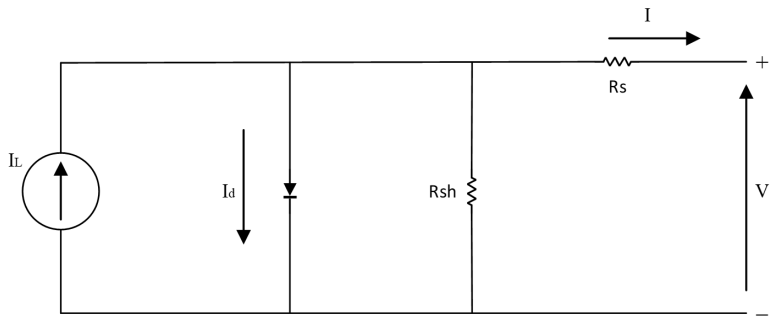

Figure 3. Single diode circuit model of PV cell

The performance of PV systems depends heavily on how they can extract power under varying environmental conditions. To achieve desired performances, DC-DC converters transform the variable DC input voltage into a stable and usable DC output voltage and implement maximum power point tracking. In this work, a DC-DC boost converter conditions the output DC voltage to match the required downstream voltage for paralleling with the other system components.

An MPPT algorithm is central to the operation of the DC-DC boost converter in this study. PV systems have a unique operating point for the maximization of output power. This operating point is not fixed; it varies with environmental conditions. To maximize the efficiency of PV systems, maximum power point tracking controllers are used to adjust their operating voltages and currents. In this work, the incremental conductance (INC) based MPPT is used to optimize the PV energy production by continuously adjusting the instantaneous and incremental conductance. A flow chart of the INC MPPT algorithm is shown in Figure 4. Mathematically, since $P = V \times I$ for a PV module, then

$$\frac{dP}{dV} = I + V\frac{dI}{dV} \tag{4}$$

At MPP, $\frac{dP}{dV} = 0$ and therefore

$$\frac{dI}{dV} = -\frac{I}{V} \tag{5}$$

In equation (5), $\frac{dI}{dV}$ is the incremental conductance and $-\frac{I}{V}$ is the instantaneous conductance.

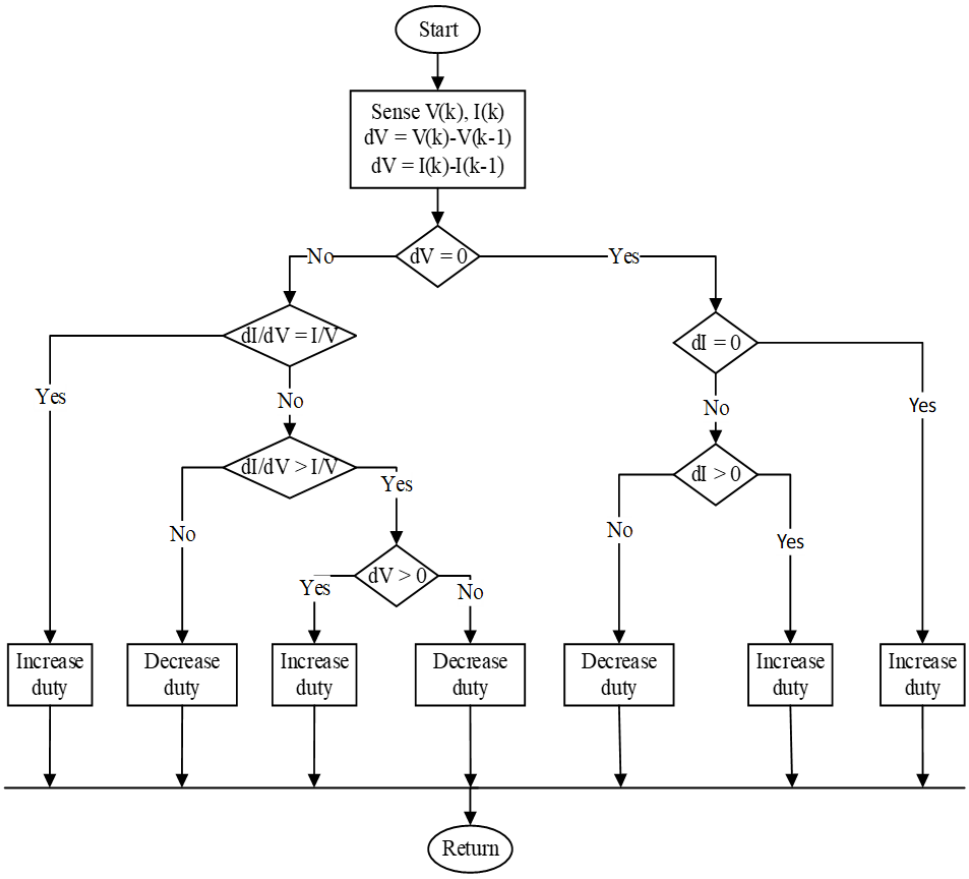

Figure 4. Incremental conductance MPPT flowchart

2. Wind Generation System

Wind energy is considered a renewable energy source with a high energy return on energy invested (EROEI) [20]. Figure 5 shows the schematic of a gearless PMSG-based wind turbine model used in this work.

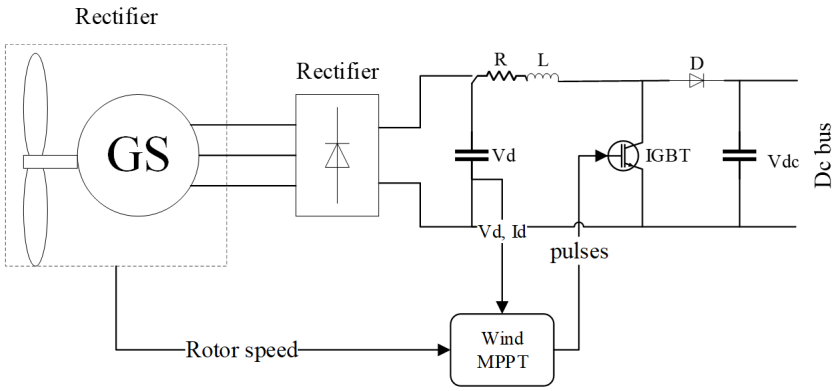

Figure 5. Wind turbine [21]

The wind turbine is connected to a DC bus through an AC-DC converter. A DC-DC boost converter is used to stabilize the DC voltage. The IGBT switch of the boost converter is controlled by an MPPT algorithm that generates a switching signal based on turbine speed, DC voltage, and current measurements. The following equation gives the mechanical output power, P_m, of the wind turbine as a function of the wind speed, V [21]:

$$P_m = c_p(\lambda, \beta)\frac{\rho A}{2}V^3 \tag{6}$$

where c_p represent the wind turbine power coefficient, ρ is the air density (kg/m^3), and A is the area swept by turbine blades. In equation (6), the turbine power coefficient, as a function of the tip speed ratio, λ, and the blade pitch angle, β, is expressed as:

$$c_p(\lambda, \beta) = c_1\left(\frac{c_2}{\lambda_i} - c_3\beta - c_4\right)e^{-c_5/\lambda_i} + c_6\lambda \tag{7}$$

with

$$\frac{1}{\lambda_i} = \frac{1}{\lambda + 0.08\beta} - \frac{0.035}{\beta^3 + 1} \tag{8}$$

and

$$\lambda = \frac{\omega R}{V} \tag{9}$$

The turbine generator model is implemented in the d-q reference frame. The model is obtained using the PMSM block in Simulink with the currents i_d and i_q reversed. For a three-phase system, the equations describing d-axis and q-axis currents and voltages of the PMSG are:

$$\frac{d}{dt}i_d = -\frac{1}{L_d}v_d - \frac{R_s}{L_d}i_d + \frac{L_q}{L_d}p\omega_m i_q \tag{10}$$

$$-\frac{d}{dt}i_q = \frac{1}{L_q}v_q - \frac{R_s}{L_q}i_q - \frac{L_d}{L_q}p\omega_m i_d - \frac{\gamma p\omega_m}{L_q} \tag{11}$$

where L_d, L_q represent the d-axis and q-axis inductances, v_d, v_q are the generator d-axis and q-axis voltages, respectively, R_s is the stator current, ω_m is the angular velocity of the generator, γ is the amplitude of induced flux, p is the number of pole pairs. The generator produces a torque given by:

$$T_e = 1.5p\left[\gamma i_q + (L_d - L_q)\, i_d i_q\right] \tag{12}$$

In this work, the round rotor model of the PMSG is used, and therefore $L_d = L_q = \frac{L_{ab}}{2}$. The parameter L_{ab} is the inductance measured between phases A and B of the generator when phase C is open. It is given by:

$$L_{ab} = L_d + L_q + (L_q - L_q)\cos\left(2\theta_e + \frac{\pi}{3}\right) \tag{13}$$

where θ_e = is the electric angle.

3. Diesel Generator

The diesel generator is modeled using a synchronous machine. The d-q axes of the machine model are shown in Figures 6(a) and (b) [22]. In the figures below, the transformed voltages are determined using the following equations [22]:

$$V_d = -i_d R_s - \omega\psi_q + \frac{d\psi_d}{dt} \tag{14}$$

$$V_q = -i_q R_s + \omega\psi_d + \frac{d\psi_q}{dt} \tag{15}$$

$$V_{fld} = i_{fld} R_{fld} + \frac{d\psi_{fld}}{dt} \tag{16}$$

Here, V_d and V_q are the d-axis and q-axis stator voltages respectively, V_{fld} is the field voltage, i_d and i_q respectively are the d-axis and q-axis stator currents, i_{fld} represent field current, R_s is the stator resistance, R_{fld} is the field resistance, ω is the rotor angular frequency, and ψ is the winding flux linkage.

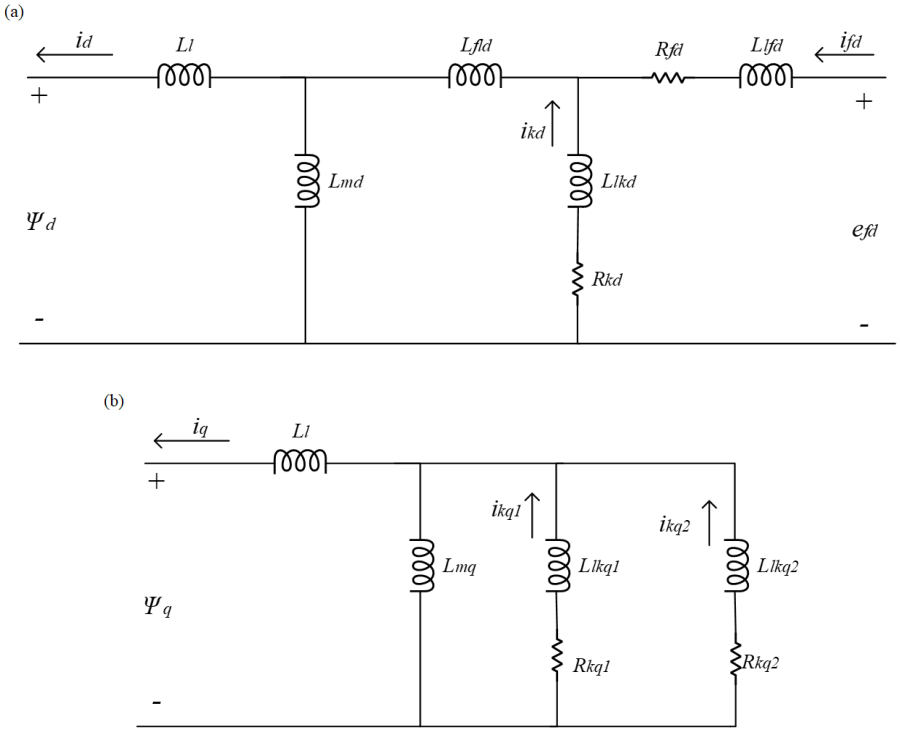

Figure 6. DG circuit model (a) d-axis (b) q-axis

4. Battery Storage System

The system employs a battery storage to supply power to the load during low or no PV and wind turbine production. It is made up of 802 Ah, 360 Vdc lead acid BESS. The initial state of charge is set to 80% with a 30-second response time. The BESS is connected to a bidirectional DC-DC converter, which regulates the battery's charging and discharging.

3. Dynamic simulation

As can be seen in Figure 7, all the power-producing components, including the battery storage system, have been connected to a single DC bus. The model is simulated in MATLAB/Simulink R2024b. The PV system consists of 21 parallel strings with 14 series-connected modules per string.

The wind farm, just as in the designed system of [18], consists of five 5kW wind turbines connected to produce 25 kW of power under ideal conditions. A 30 kW (37.5 kVA) diesel generator serves as backup power. Finally, a 360 V 802 Ah battery bank supports the other power-producing components during periods of low production. The initial state of charge is set to 80%. Below is a table summarizing all the components' parameters used in this work (Table 2).

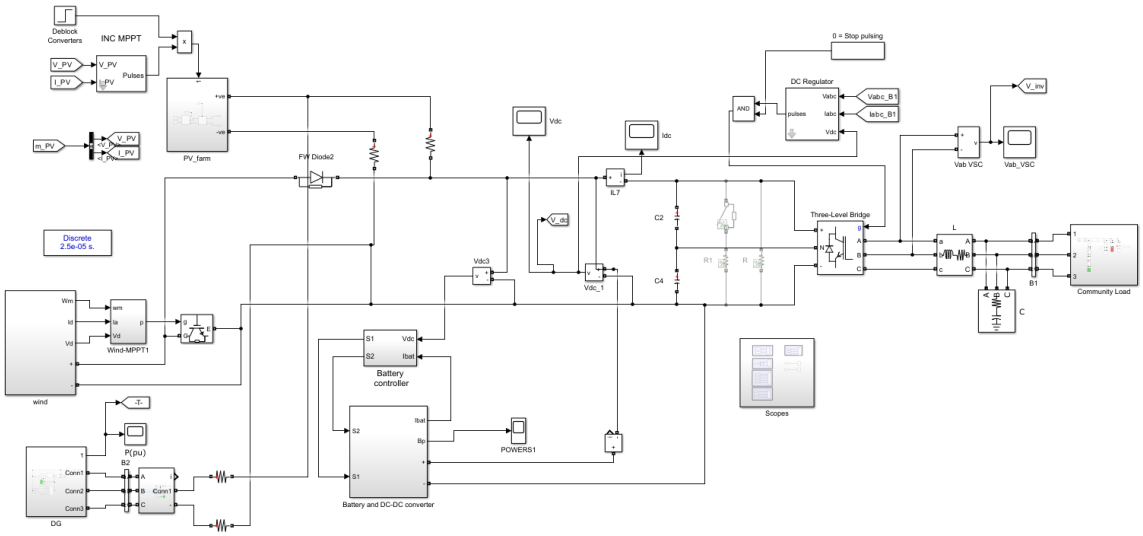

Figure 7. Complete system dynamic model in Simulink

Table 2. Components' parameters

PV	
Model	Jinko Solar JKM350-72
Number of strings	21
Number of series-connected modules per string	14
Wind Turbine (Parameters for 1 component)	
Nominal mechanical power (W)	5,000
Base electrical power (VA)	5,000/0.9
Base wind speed (m/s)	12
PMSG (parameters for 1 component)	
Number of poles	10
Stator phase resistance (Ω)	0.425
Inductances L_d, L_q (H)	0.0082, 0.0082
Flux linkage (V·s)	0.433
Inertia (kgm^2)	0.01197
Viscous damping (N·m·s)	0.001189
Diesel Generator	
Nominal power (VA)	37,500
Voltage (V)	380 V
Frequency (Hz)	50
BESS	
Nominal power (kWh)	289 (2.408 kWh × 120 units)
Voltage (V)	360 V (12 V × 30)
Capacity (Ah)	802(201 Ah × 4 in parallel)

4. Simulation results

This section presents the dynamic simulation results for the Azizakpe community. The simulation was run for 2.5 seconds on an Intel Core i5 personal computer. Additionally, the simulation was configured with a time step of 2.5 microseconds and a variable step solver (ode23tb). The initial conditions were set to zero, and the system was assumed to operate under steady-state conditions.

Figure 8 shows the voltage and current generation from the solar system. The simulation is carried out for three different insolation levels: 500 W/m^2 from 0 to 0.4 s, 800 W/m^2 from 0.4 to 1s, and 1,000 W/m^2 from 1 s to the end of the simulation, to observe the system's response to varying solar irradiance. At the beginning of the simulation, when the irradiance is at 500 W/m^2, the outputs of both voltage and current of the PV array are relatively low. As irradiance increases to 800 W/m^2 at 0.4 s, the PV current and voltage rise accordingly. A further increase to 1,000 W/m^2 at 1 s leads to the highest observed current and voltage output.

Throughout each transition, a transient waveform fluctuation in voltage and current is observed, indicating the system's response to the changing insolation levels. This can be seen at times 0.4 s and 1 s in Figure 8. These transient fluctuations are significant, as they reflect the behavior of the MPPT implemented in the system. The oscillations around each new steady-state value suggest that the MPPT controller is actively adjusting the operating point of the PV array to achieve maximum power extraction.

Figure 9 shows the wind turbine's output power under varying wind speeds. It can be observed that the turbine produces no power until about 0.35 s. Beyond 0.35 s, the output power increases sharply and stabilizes. This stability is due to the pitch control system implemented in this work. The pitch mechanism adjusts the blade angles to regulate rotational speed and maintain steady power generation. The effectiveness of this system ensures that, even with the changes in wind speed, the output power remains within a desired range, thereby optimizing energy capture.

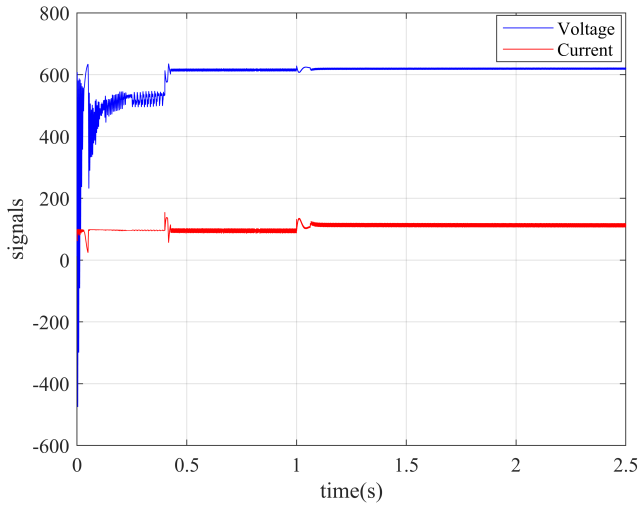

Figure 8. PV voltage and current

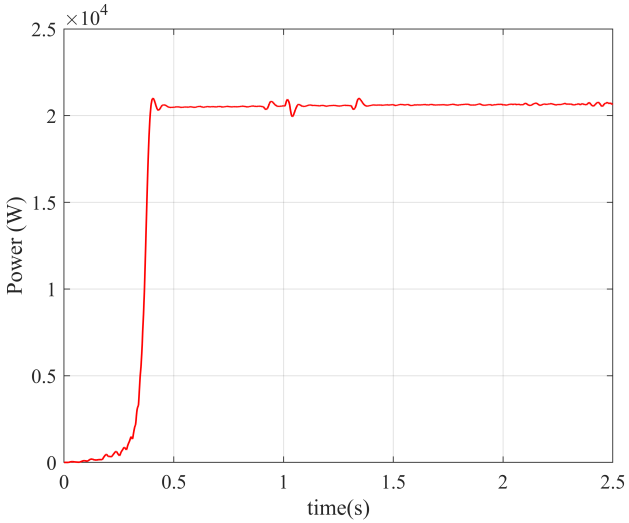

Figure 9. Wind turbine power

The turbine's output phase voltage and line current waveforms are shown in Figures 10 and 11, respectively. The waveforms show that the turbine is fairly regulated to produce stable current and voltage waveforms.

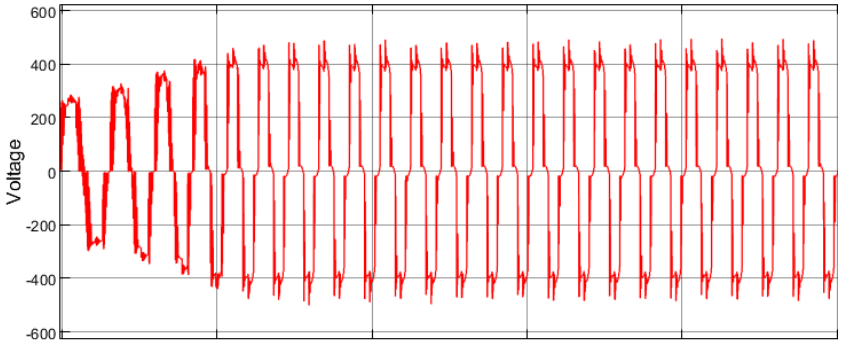

Figure 10. Wind turbine AC voltage

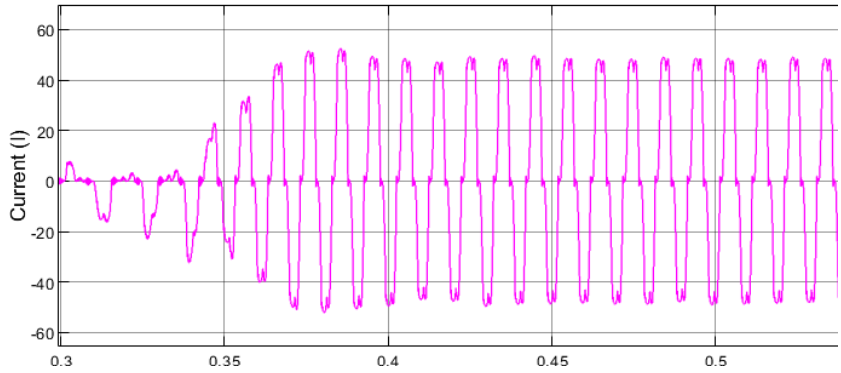

Figure 11. Wind turbine AC current

Figures 12 and 13 present the turbine's DC voltage and current, respectively. The rectified voltage waveform in Figure 12 demonstrates a relatively smooth DC output with minor ripples, indicating effective rectification and filtering. Similarly, the rectified current waveform in Figure 13 shows a consistent current draw. The near-stable and ripple-free DC voltage and current waveforms obtained are essential for supplying the DC bus downstream.

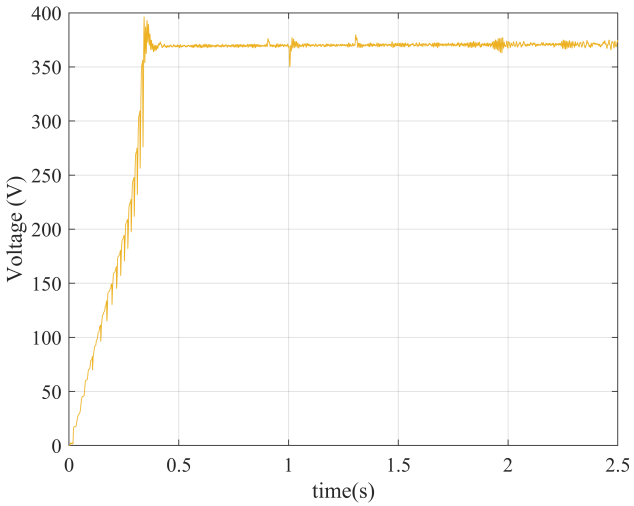

Figure 12. Wind turbine rectified voltage

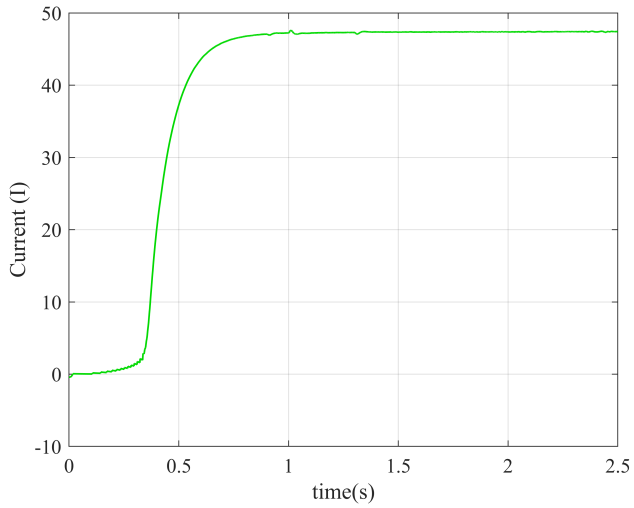

Figure 13. Rectified wind turbine current

The DG's output power, mechanical input power, and rotor speed are shown in Figures 14, 15, and 16, respectively. It is observed in Figure 14 that the DG's output power rises from 0.1 pu to 0.6 pu at the end of the simulation. Figure 15 shows the mechanical input power, which exhibits an initial overshoot reaching nearly 0.22 pu, followed by rapid oscillations that dampen out and stabilize at a low steady-state level. In Figure 16, the rotor speed temporarily exceeds the nominal value 1

pu between approximately 0.2 and 1.18 s, before gradually settling around 1 pu thereafter. This demonstrates the transient behavior during synchronization and eventual speed regulation during normal operating conditions.

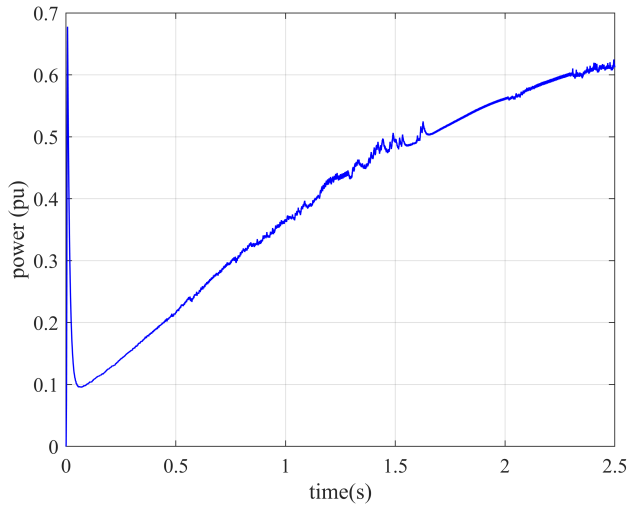

Figure 14. DG output power (pu)

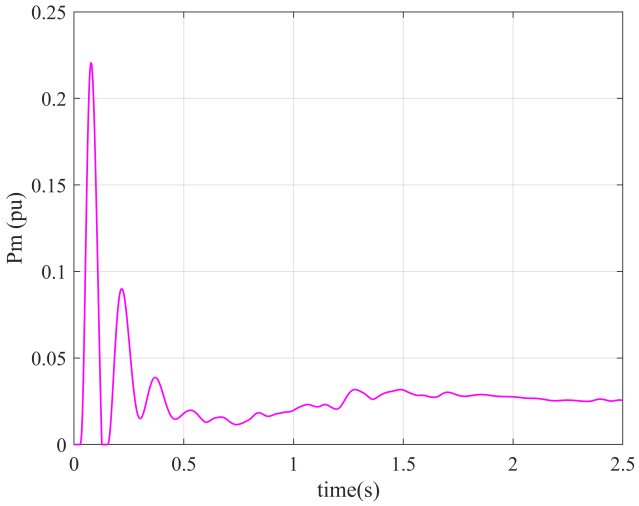

Figure 15. DG input mechanical power (pu)

Figure 17 shows the battery's state of charge, current, and voltage waveforms. The negative current waveform indicates the battery system is charging during the simulation. The battery's voltage is well maintained at 360 V, and the SoC is at 80%.

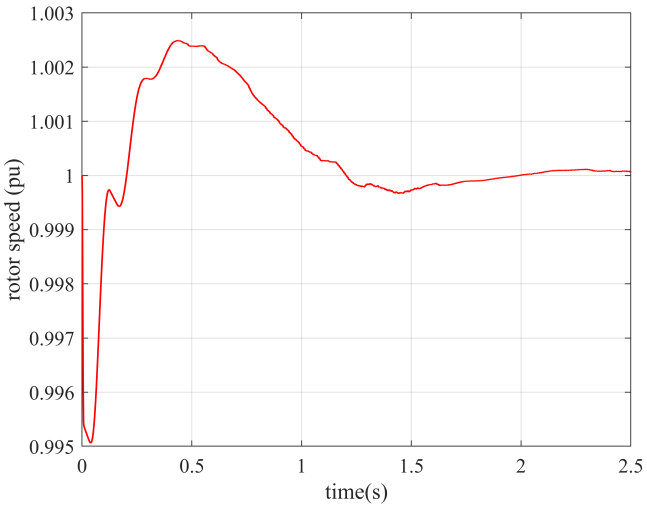

Figure 16. DG rotor speed (pu)

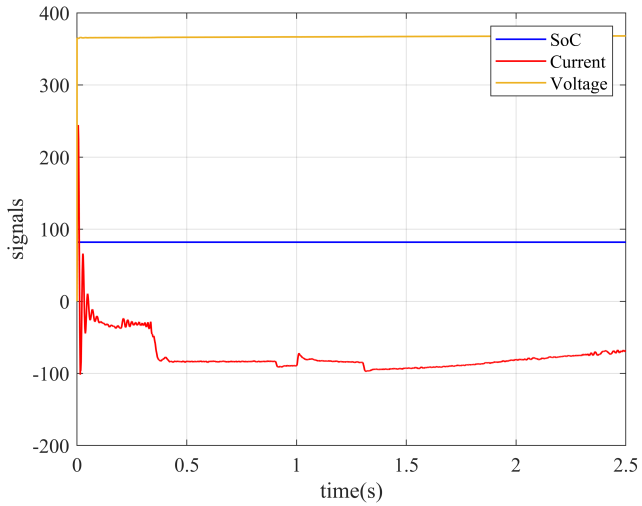

Figure 17. Battery SoC, current, and voltage waveforms

In this work, the system is designed to interface with a battery system of 360 V. To ensure proper operation, the output DC voltage is controlled to match the battery's voltage. Figure 18 shows the system's output DC voltage waveform. At the beginning of the simulation, it is observed that the voltage waveform fluctuates around the 360 V mark. However, the system's DC voltage stabilizes at 360 V after about 0.1 s. The system's DC current is also presented in Figure 19. From the DC voltage waveform, it is observed that the system is fairly balanced and operates satisfactorily under normal conditions.

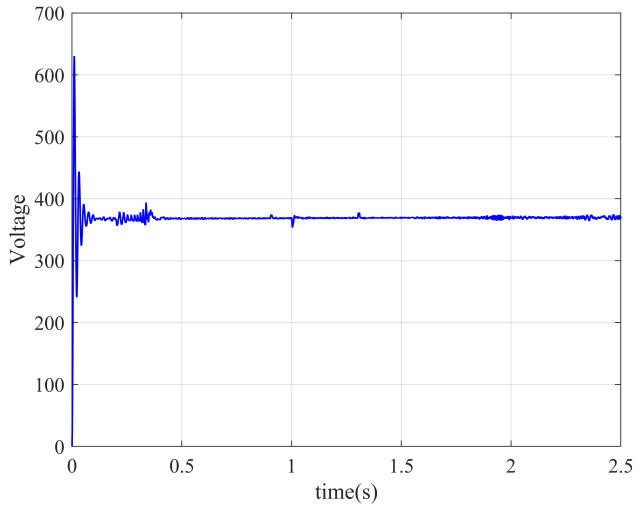

Figure 18. System DC voltage

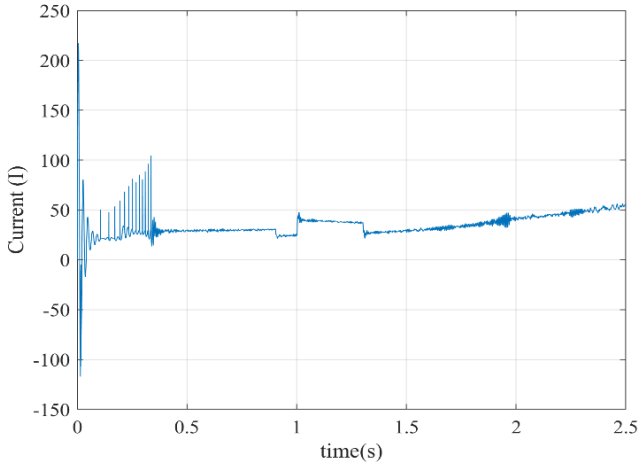

Figure 19. System DC current

This work is simulated under different load levels to evaluate the dynamic response. Circuit breakers are used to switch the different load levels. A load of 8.2 kW is applied between 0.2 and 0.9 s, followed by the system's peak load of 41.6 kW as calculated in [18] between 1 and 1.3 s. The average load of 11.63 kW is applied between 2 and 2.5 s. In between these times, there is a load of 20 kW. These step changes in load levels allow for a precise observation of the system's transient response. In Figures 20–22, the resulting waveforms reflect the system's load current and voltage behavior across a range of operating scenarios, clearly indicating stable output voltage for changing load conditions.

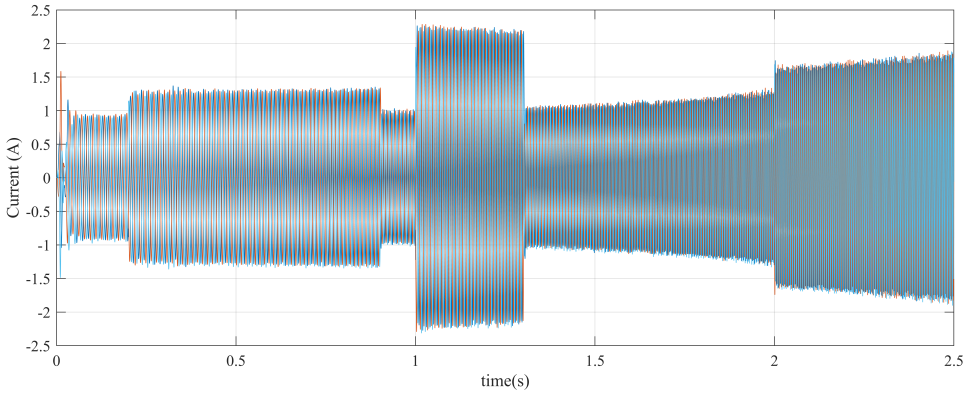

Figure 20. Load current waveform to load changes at 0.2 s, 1 s, 1.3 s and 2 s for 5.5 kW, 41.6 kW, 20 kW, and 10 kW, respectively

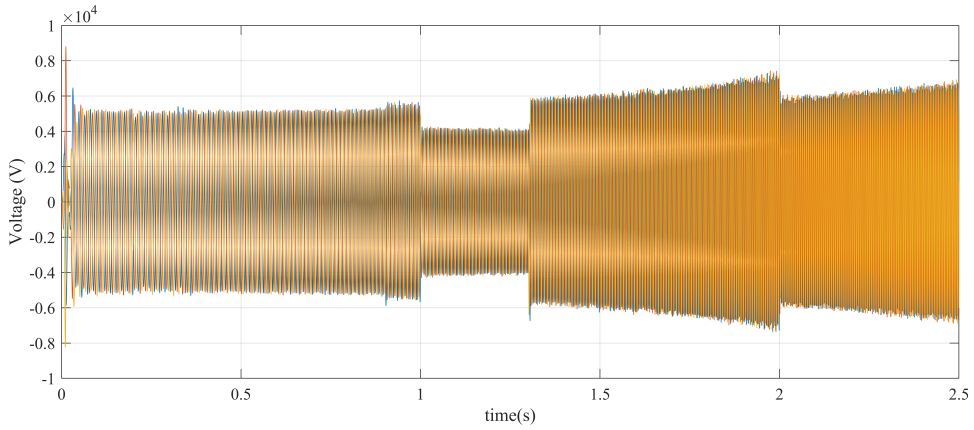

Figure 21. Load voltage response to load changes at 0.2 s, 1 s, 1.3 s and 2 s for 5.5 kW, 41.6 kW, 20 kW, and 10 kW, respectively

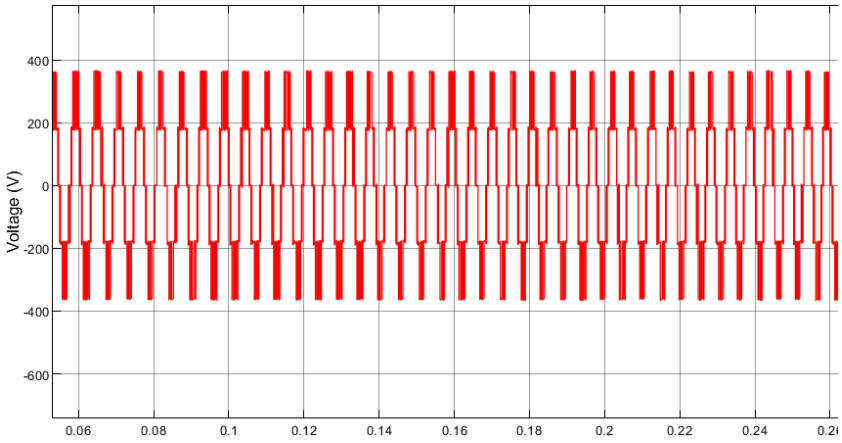

Figure 22. Inverter output voltage

5. Conclusion

This study presented a detailed dynamic modeling and simulation of a DC microgrid for a remote community in Ghana using MATLAB/Simulink. MPPT maximizes energy extraction from the PV and wind turbine systems. In the case of the PV, an incremental conductance MPPT algorithm is used due to its effectiveness in minimizing oscillations at the MPP. MPPT based on wind speed measurement is used for the wind turbine. Finally, a DC-DC converter controls the battery's charging and discharging. The simulation was conducted for different operating scenarios: varying solar irradiance, wind speeds, and load levels. The results from the simulation demonstrated stable DC voltage regulation across varying load conditions. In addition, the inverter maintained a consistent output voltage waveform. These results collectively validate the system's dynamic design and ability to provide stable and reliable power for the remote community.

Building on the dynamic simulation results, which utilized idealized components from Matlab/Simulink, future work will involve implementing a microgrid supervisory control and data acquisition (SCADA) system. The work will use laboratory solar, wind, diesel generator, and battery components. This will enable real-time monitoring, control, and data acquisition to enhance further the operation, reliability, and management of the DC microgrid for the community.

Acknowledgement

This study was supported by the Discovery Grants of the Natural Sciences and Engineering Research Council of Canada (NSERC).

Conflicts of interest

The authors declare no competing financial interest.

References

[1] M. Naderi, Y. Khayat, Q. Shafiee, F. Blaabjerg, and H. Bevrani, "Dynamic modeling, stability analysis and control of interconnected microgrids: a review," *Applied Energy*, vol. 334, 2023, https://doi.org/10.1016/j.apenergy.2023.120647.

[2] D. Espin-Sarzosa *et al.*, "Microgrid modeling for stability analysis," *IEEE Transactions on Smart Grid*, vol. 15, no. 3, pp. 2459-2479, 2024, https://doi.org/10.1109/TSG.2023.3326063.

[3] E. Hossain, R. Perez, A. Nasiri, and S. Padmanaban, "A comprehensive review on constant power loads compensation techniques," *IEEE Access*, vol. 6, pp. 33285-33305, 2018, https://doi.org/10.1109/ACCESS.2018.2849065.

[4] S. P. Nandanoori, S. Kundu, W. Du, F. K. Tuffner, and K. P. Schneider, "Distributed small-signal stability conditions for inverter-based unbalanced microgrids," *IEEE Transactions on Power Systems*, vol. 35, no. 5, pp. 3981-3990, 2020, https://doi.org/10.1109/TPWRS.2020.2982795.

[5] O. Bassey, K. L. Butler-Purry, and B. Chen, "Dynamic modeling of sequential service restoration in islanded single master microgrids," *IEEE Transactions on Power Systems*, vol. 35, no. 1, pp. 202-214, 2020, https://doi.org/10.1109/TPWRS.2019.2929268.

[6] M. Yousaf, K. Muttaqi, and D. Sutanto, "An investigative analysis of the protection performance of unbalanced distribution networks with higher concentration of distributed energy resources," *IEEE Transactions on Industry Applications*, vol. 58, no. 2, pp. 1771-1782, 2022, https://doi.org/10.1109/TIA.2022.3145778.

[7] L. G. Meegahapola, D. Robinson, A. P. Agalgaonkar, S. Perera, and P. Ciufo, "Microgrids of commercial buildings: strategies to manage mode transfer from grid connected to islanded mode," *IEEE Transactions on Sustainable Energy*, vol. 5, no. 4, pp. 1337-1347, 2014, https://doi.org/10.1109/TSTE.2014.2305657.

[8] R. K. Sharma and S. Mishra, "Dynamic power management and control of a PV PEM fuel-cell-based standalone ac/dc microgrid using hybrid energy storage," *IEEE Transactions on Industry Applications*, vol. 54, no. 1, pp. 526-538, 2018, https://doi.org/10.1109/TIA.2017.2756032.

[9] L. M. Castro, C. Ramírez-Ramos, R. Tapia-Olvera, and D. Guillén, "Dynamic modelling framework for the analysis of fair-sized DC microgrids," *International Journal of Electrical Power and Energy Systems*, vol. 158, p. 109912, 2024, https://doi.org/10.1016/j.ijepes.2024.109912.

[10] E. Jacob and H. Farzaneh, "Modeling and performance evaluation of hybrid photovoltaic thermal, wind, and battery microgrids using optimization and dynamic simulation," *Scientific Reports*, 2025, https://doi.org/10.1038/s41598-025-95149-w.

[11] K. M. Bhargavi, N. S. Jayalakshmi, D. N. Gaonkar, A. Shrivastava, and V. K. Jadoun, "A comprehensive review on control techniques for power management of isolated DC microgrid system operation," *IEEE Access*, vol. 9, pp. 42162-42185, 2021, https://doi.org/10.1109/ACCESS.2021.3060504.

[12] Z. Zhao *et al.*, "Distributed robust model predictive control-based energy management strategy for islanded multi-microgrids considering uncertainty," *IEEE Transactions on Smart Grid*, vol. 13, no. 3, pp. 2107-2120, 2022, https://doi.org/10.1109/TSG.2022.3147370.

[13] M. I. Juma, B. M. M. Mwinyiwiwa, C. J. Msigwa, and A. T. Mushi, "Design of a hybrid energy system with energy storage for standalone DC microgrid application," *Energies*, vol. 14, no. 18, p. 5994, 2021, https://doi.org/10.3390/en14185994.

[14] I. Hussain *et al.*, "Active power control of autonomous hybrid power system using two degree of freedom PID controller," *Energy Reports*, vol. 8, pp. 973-981, 2022, https://doi.org/10.1016/j.egyr.2022.05.202.

[15] B. Jiang and M. T. Iqbal, "Dynamic modeling and simulation of an isolated hybrid power system in a rural area of China," *Journal of Solar Energy*, vol. 2018, p. 5409069, 2018, https://doi.org/10.1155/2018/5409069.

[16] R. P. Nair and K. Ponnusamy, "Modeling and simulation of autonomous DC microgrid with variable droop controller," *Applied Sciences*, vol. 15, no. 9, p. 5080, 2025, https://doi.org/10.3390/app15095080.

[17] E. Jacob and H. Farzaneh, "Dynamic modeling and experimental validation of a standalone hybrid microgrid system in Fukuoka, Japan," *Energy Conversion and Management*, vol. 274, p. 116462, 2022, https://doi.org/10.1016/j.enconman.2022.116462.

[18] G. Atinkum, M. T. Iqbal, and J. E. Quaicoe, "Techno-economic design and sensitivity analysis of a DC microgrid for a remote community: a case study in Ghana," *Journal of Electronics and Electrical Engineering*, vol. 4, no. 1, pp. 357-378, 2025, https://doi.org/10.37256/jeee.4120256509.

[19] M. Kumar Singla *et al.*, "Mathematical modeling for solar cell optimization: evaluating sustainability with different diode configurations," *IEEE Access*, vol. 12, pp. 93802-93822, 2024, https://doi.org/10.1109/ACCESS.2024.3424416.

[20] R. L. Rana, M. Lombardi, P. Giungato, and C. Tricase, "Trends in scientific literature on energy return ratio of renewable energy sources for supporting policymakers," *Administrative Sciences*, vol. 10, no. 2, p. 21, 2020, https://doi.org/10.3390/admsci10020021.

[21] K. Tazi, M. F. Abbou, and F. Abdi, "Performance analysis of micro-grid designs with local PMSG wind turbines," *Energy Systems*, vol. 11, no. 3, pp. 607-639, 2020, https://doi.org/10.1007/s12667-019-00334-2.

[22] *IEEE Guide for Synchronous Generator Modeling Practices and Parameter Verification with Applications in Power System Stability Analyses*, IEEE Standard 1110-2019, 2020.